Electronic Supplementary Material (ESI) for Physical Chemistry Chemical Physics.

Supporting information

Interface/defect-tunable macro and micro photoluminescence behaviours of Trivalent europium ions in electrospun ZrO_2/ZnO porous nanobelts

Yanzhe Mao,[a] Jinglong Bai,[a] Mingxiang Zhang,[a] Hao Zhao,[a] Jiayi Chen,[a] Zhenyu Yang, [a] Xiuyun Gu, [a] Gengzhi Sun,[b] Xiaojun Pan,[a] Zhenxing Zhang,[a] Jinyuan Zhou,*,[a] Erqing Xie*,[a]

[a]School of Physical Science and Technology, Lanzhou University, 222 South Tianshui Road, Lanzhou 730000, People's Republic of China

[b]Key Laboratory of Flexible Electronics & Institute of Advanced Materials, Jiangsu National Synergetic Innovation Center for Advanced Materials, Nanjing Tech University, 30 South Puzhu Road, Nanjing 211816, People's Republic of China

Corresponding Authors: zhoujy@lzu.edu.cn; xieeq@lzu.edu.cn

1) SEM images

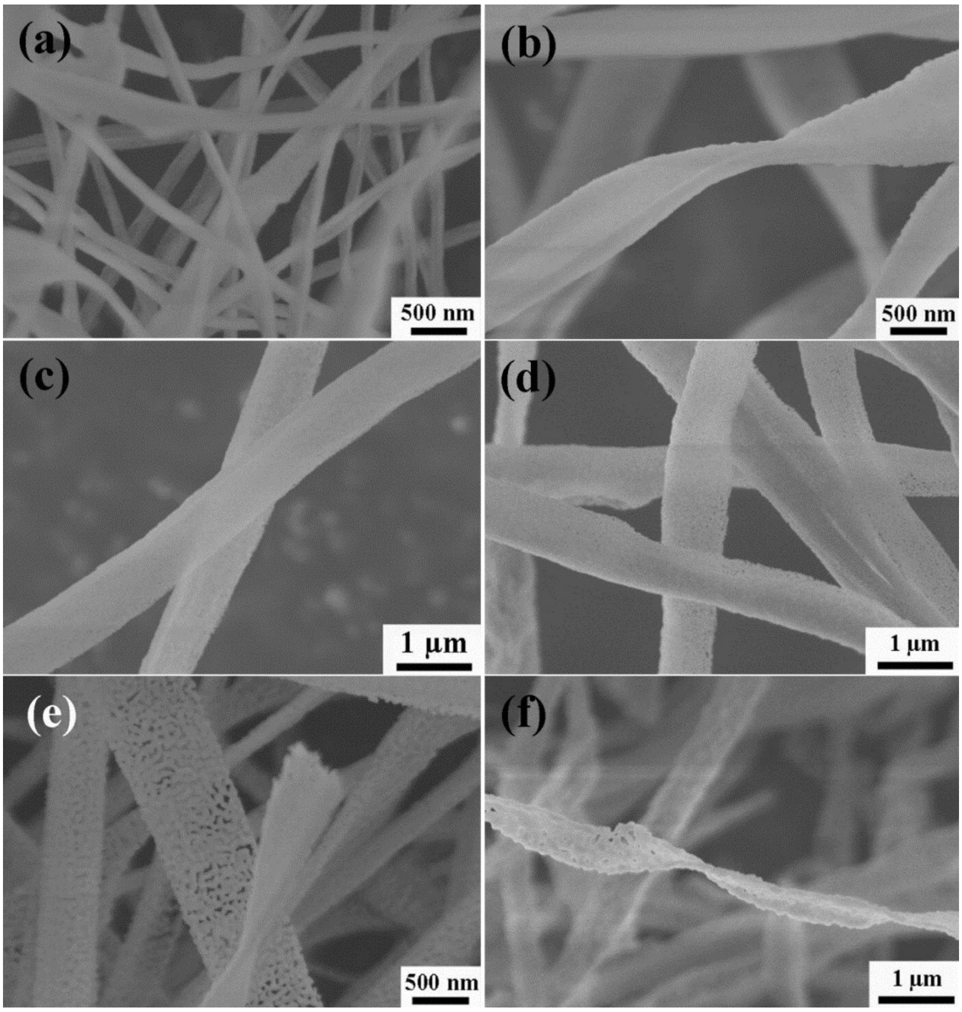

Figure S1 SEM images of ZrO_2/ZnO: Eu^{3+} composites annealed at different temperatures in air: (a) 500 °C, (b) 600 °C, (c) 700 °C, (d) 800 °C, (e) 900 °C, and (f) 1000 °C.

The ZrO_2/ZnO: Eu nanostructures with Zr/Zn mole ratio of 3:1 annealed at 500 ºC are not of the traditional fibrous shape, some of them have changed into nanobelts, some of them are in a transition state, and a few of them remain fibrous shape. The sizes of these composite nanobelts are about 200-500 nm. More details of the formed nanobelts can be viewed from the samples annealed at 600 ºC. Most of the composite nanofibers in the samples are changed into nanobelts with width of ~ 600-700 nm and thickness of ~dozen nanometers. With increasing the annealing temperature from 800 to 1000 °C, the smooth compact nanobelts gradually change into more porous and coarser ones.

2) XRD patterns

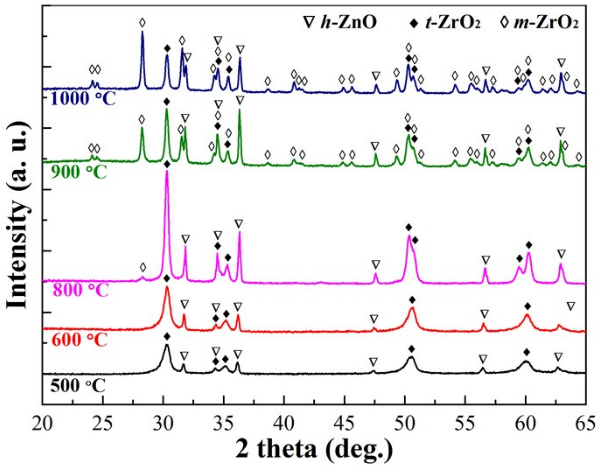

Figure S2 XRD patterns of undoped ZrO_2/ZnO composites annealed at different temperatures.

As shown, the XRD spectrum of the samples annealed at 500 ºC reveals two components, i.e. tetragonal ZrO_2 (t-ZrO_2) and hexagonal ZnO (h-ZnO). The peaks at 2θ = 30.32º, 34.30º, 35.11º, 50.53º, and 60.07º marked with ♦ can be assigned to <101> , <002>, <110>, <112>, and <211> lattice planes of t-ZrO_2 (JCPDS No. 42-1164), and the ones at 31.69º, 34.30º, 36.16º, 47.41º, 56.47º, and 62.66º marked with ∇ to <100>, <002>, <101>, <102>, <110>, and <103> lattice planes of h-ZnO with a wurtzite structure (JCPDS No. 36-1451). With the annealing temperature increasing from 500 to 800 ºC, the crystallinity level of t-ZrO_2 increases linearly. And at 800 ºC, two obvious changes can be observed in the spectrum. One change is a new diffraction peak arising at 2θ=28.30º, which corresponds the <-111> lattice plane of m-ZrO_2 (JCPDS No. 65-1022). This indicates that the t-ZrO_2 phase begins to transform into m-ZrO_2 one at 800 ºC. The other change is that the two broad diffraction peaks of t-ZrO_2 at 2θ= ~50º and ~60º respectively begin to split into two components. And the peaks locating at 50.36º and 50.80º correspond to the <112> and <200> lattice plane, respectively, and the ones at 59.46º and 60.25º to the <103> and <211> lattice plane of t-ZrO_2, respectively. Further increasing the temperature to 900 ºC, even to 1000 ºC, all diffraction peaks of m-ZrO_2 phase appear in the spectra, and the intensities of diffraction peaks of t-ZrO_2 greatly decrease. The diffraction peaks at

2θ = 24.13º, 24.52º, 28.28º 31.51º, 34.22º, 34.55º, 35.40º, 38.66º, 40.83º, 41.27º, 41.49º, 44.92º, 45.62º, 49.36º, 50.27º, 50.71º, 51.31º, 54.16º, 55.50º, 56.01º, 57.27º, 59.43º, 59.93º, 60.22º, 61.45º, 62.12º, 63.10º, and 64.29º marked with ◊ well correspond to <011>, <110>, <-111>, <111>, <002>, <020>, <200>, <021>, <-211>, <102>, <-121>, <112>, <211>, <022>, <220>, <-122>, <-221>, <202>, <013>, <130>, <310>, <131>, <-222>, <-302>, <113>, <-213>, <311>, and <032> lattice planes of *m*-ZrO_2 (JCPDS No. 65-1022). Moreover, via fitting analysis of the strongest peaks of *m*-ZrO_2, *t*-ZrO_2 and *h*-ZnO, the volume fraction of *m*-ZrO_2 phase reaches about 70% when the annealing temperature increases up to 1000 ºC. The peak position of each component monotonously shifts from lower degree to higher degree with increasing annealing temperature, e.g., the <101> peak of *t*-ZrO_2 slightly shift from 30.26º to 30.31º, the <101> peak of *h*-ZnO slightly from 36.15º to 36.35º.

3) IR spectra

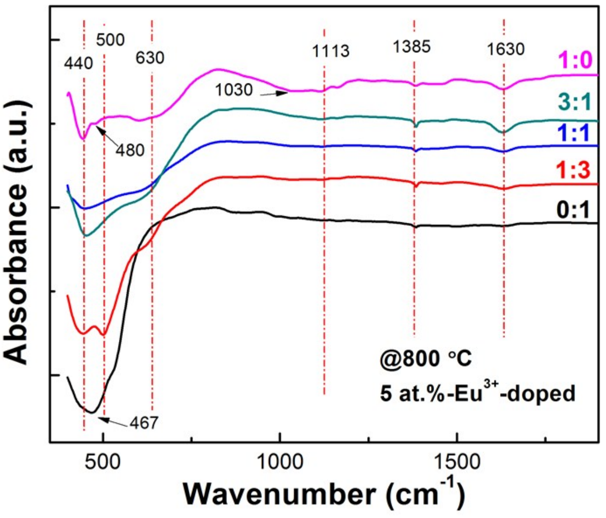

Fig. S3 IR spectra of ZrO_2/ZnO: Eu^{3+} with different Zr-Zn ratios.

For all the samples, the main absorption bands appear between 400 and 800 cm^{-1}. The Eu^{3+}-doped ZnO (0:1) samples show one main absorption band at 467 cm^{-1}, which corresponds to ν(Zn-O) bond.[1] Once ZrO_2 was incorporated, the main one absorption has been split into two components locating at 440 and 500 cm^{-1}, which correspond to ν (Zr-O) and ν (Zn-O) bonds, respectively. The absorption band of the

ZrO_2 components at 440 cm^{-1} can be assigned to the symmetric Zr– O–Zr stretching mode related with t-ZrO_2 phase.[2] And there also arises a new broad and weak absorption band at ~630 cm^{-1} in the FTIR spectra, which is related to the coupled asymmetric Zr–O–Zr stretching mode from the *m*-ZrO_2 phase, indicating that a phase change occurs in the ZrO_2 components annealed at 800 ºC.[3, 4] This is different from the XRD observation about Eu^{3+}-doped samples, in which the m-ZrO_2 components can form only during 1000 annealing process. This difference could be due to the high sensitivity in characterization of chemical bonds in the samples from FTIR tests. Further increase the content of ZrO_2 components (1:1 and 3:1), the main absorption bands change into one broad and poor resolved absorption band with a broad shoulder. The strong absorption band at 440 cm^{-1} corresponds to the ν(Zr-O) band from t-ZrO_2 components, and the shoulder band at 630 cm^{-1} to m-ZrO_2 components. While the absorption band corresponding to ν (Zr-O) band from ZnO components is integrated with the one from t-ZrO_2 components, indicating that the symmetry of the structure is reduced markedly. Moreover, the intensities of low absorption bands at 1385 and 1630 cm^{-1} increase with increasing the content of ZrO_2, and correspond to ν_s(–OCH) and ν(C=O) stretching modes.[2] These bands are related to the physically absorbed hydroxyl groups and/or the organic components used during the electrospinning processes. These bands appear in all IR spectra of ZrO_2-ZnO composites, even when the films annealed at 1000 ºC (Figure 8(b)). As for ZrO_2: Eu^{3+} samples (1:0), there arises another new broad and poor resolved absorption bands in the range of 1000-1200 cm^{-1}, which might be related with the remaining C–O–C groups, indicating that the obtained ZrO_2:Eu^{3+} samples are highly insufficient of oxygen and contain increasing VOs.[5, 6]

4) UV-Vis spectra

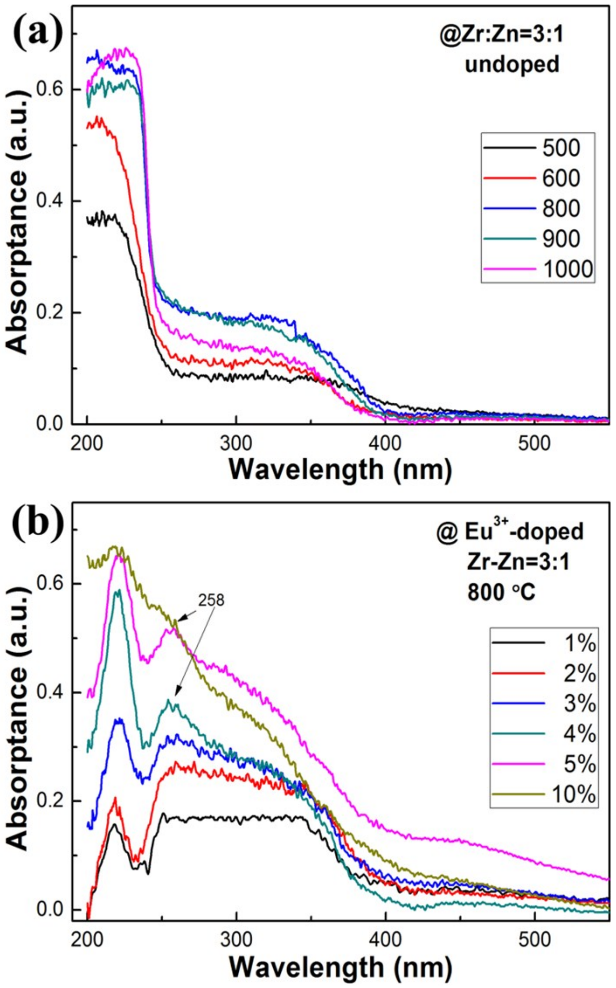

Figure S4 UV-Vis spectra of (a) undoped ZrO_2/ZnO composites annealed at different temperatures and (b) ZrO_2/ZnO: Eu^{3+} composites doped with different Eu^{3+} ion contents.

To make clear the origin of the absorption peak centered at 258 nm in UV-Vis spectra, we also tested the UV-Vis spectra of the undoped ZrO_2/ZnO composites with Zr-Zn ratio of 3:1 annealed at different temperatures, as shown in Fig. S4(a). The UV-Vis spectra are also comprised of two absorption bands, i.e., 200-250 nm and 250-380 nm. The biggest difference compared to those from the doped samples is that the curve shape almost shows no change with increasing the temperature from 500 to 1000 ºC, and there is no absorption peak around 258 nm. The absorption intensity in the range of 200-250 nm monotonously increases with the annealing temperatures, which is due to the highly improved crystallinity of the samples. While the absorption intensity in the range of 250-380 nm initially increases with temperature increasing from 500 to 800 ºC, and then slightly decreases with further increasing temperature from 800 to 1000 ºC. Similar with the above analysis, this decrease in absorption can also be due to the decrease of oxygen defects caused by the separation out of ZnO components.

To further make clear the origin of the absorption peak centered at 258 nm, we further tested the UV-Vis spectra of the ZrO_2/ZnO: Eu^{3+} composites doped with different Eu^{3+} ion contents. In this case the Zr-Zn ratio is kept at 3:1, and the annealing temperature is set as 800 ºC. As shown in Fig. 5(g), The UV-Vis spectra are also comprised of two absorption bands, i.e., 200-250 nm and 250-380 nm, and their gross absorption increases with the increasing doping content of Eu^{3+} ions, especially the absorption in the range of 250-380 nm. At the same time, the intensity of the absorption peak centered at 258 nm also increase with increasing the Eu doping contents from 1% to 5%; and further doping cannot greatly increase the absorption intensity but largely influence the absorption edge from ZrO_2 components. These tests indicate that this 258-nm peak is caused by the absorption from Eu-related components in the samples.

5) PL undoped ZrO2/ZnO composites

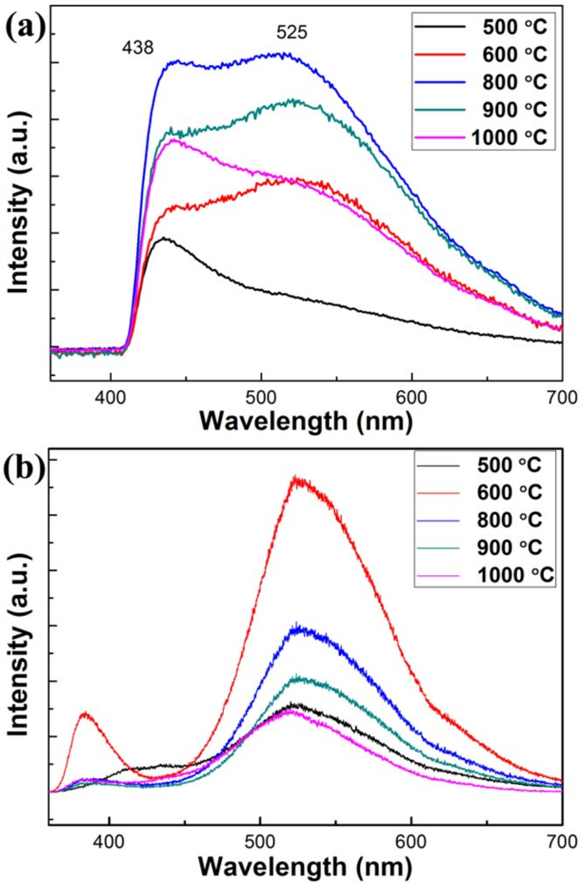

Fig. S5 (a) macro- (b) micro- PL spectra of undoped ZrO_2/ZnO composites annealed at different temperatures.

To further investigate the light emissions from defects of the surface and inner part of the nanobelts, we compared the macro- and micro-PL from the undoped ZrO_2/ZnO composites with Zr-Zn ratio of 3:1 annealed at different temperatures. As shown in Fig. 7(a), all PL spectra are comprised of two broad emission peaks, which centered at 438 nm and 525 nm, respectively. From our previous work,[7-10] these two bands could be due to the formed VOs. Moreover, Singh have assigned the peak around 500 nm has been attributed to the defects present in the ZnO lattice.[11] Wang et al. also thought that the broad defect-related green emission (GE) band centered at ∼510 nm has often been ascribed to the radiative recombination of photogenerated holes with electrons induced by the oxygen vacancies.[12] Tay et al. considered the green emissions to oxygen vacancies distributed beneath the surface of ZnO.[13] Dileep et al. reported that green emission is due to the oxygen defect states in the bandgap just below the conduction band.[14] Bayan et al found the oxygen interstitial defect related emission centered at 535 nm.[15] Du et al also observed a weak and broad green emission band centering at around 536 nm, which is resulted from the presence of singly ionized oxygen vacancies or interstitial zinc ions (or other point defects).[16] And Chen et al. have observed a strong green emission band located at ~515 nm, which is corresponded to oxygen vacancy (VO) and denoted as deep level emission.[17] So, it can be deduced that the 525-nm green emission is mainly due to the VOs in the ZnO. As for the 438 nm emission, most researchers considered it to the blue emission from VOs in ZrO_2. Stojadinović found that the PL band centered at about 490nm is associated with oxygen vacancy defects.[18] Sidhu et al. found that for Zirconia nanoparticle annealed at 600 ºC, the PL peak at 423 nm (2.93 eV) may be from some mid trap states or oxygen vacancies.[19] Nikiforov et al. stated that shallow traps caused by oxygen vacancies and impurity titanium ions contribute to emission at 480 nm. [2, 20] And Perevalov and Villa groups concluded that the 2.7 eV blue luminescence excited near 5.2 eV in a zirconium oxide film is associated with the oxygen vacancy. [21, 22] besides, Gao et al. thought that the blue emission of the sample might be likely linked to the radiative defects at the interface of the components of ZnO urchins, or the existence of interstitial zinc in ZnO lattices.[23] And Park et al. also contributed the peaks at 439 and 508 nm in the thin rods were attributable to the recombination of the interstitial zinc (Zn_i) with zinc vacancies (Vzn) and the combination of singly charged oxygen vacancies (Vo^+) with photo-excited holes in the valence band, respectively.[24] In brief, the 525-nm green emission is mainly due to the V_Os in ZnO components, while the blue emission at 438 nm might be due to the interfacial V_Os (or surficial V_Os) between two components (ZnO and ZrO_2).

The intensities of both emission increase with temperature increasing from 500 to 800 ºC, and then slightly decrease with further increasing temperature from 900 to 1000 ºC. Based on the XRD analysis above, this trend can be explained as following: at the initial stage, the crystallinity level of both ZnO and ZrO_2 components increase with the annealing temperature from 500 to 800 ºC. During this process, the oxygen atoms will escape more and more with the increasing temperatures, leading to the increase in surficial VOs (S-V_Os). And at the same time, the grain size of ZrO_2 and ZnO also increase with the temperature, which leads to the increase of the inner stress and results into the increase of B-V_Os). Further increase the temperature, the ZnO begin to separate out from the ZrO_2 matrix, which relieves the inner stress and leads to the decrease the B-V_Os. Thus, it is assumed that the 438 nm emission is caused by the S-V_Os, and the 525-nm emission is associated with B-V_Os. For comparison, the micro PL spectra show very large difference in shape (Fig. 7(b)). There are two emission peaks centered at 380 nm and 525 nm, and the 525-nm emissions are much higher than the 380-nm ones. The 380-nm emission is caused by the near band edge of ZnO components [25]. And, the 438-nm emissions disappear from all micro-PL spectra. This observation proves our assumption above that the 438-nm emissions are mainly associated with the S-V_Os.

On the other hand, the intensities of the 525-nm emissions increase with temperature increasing from 500 to 600 ºC, and then decrease gradually with further increase temperature from 800 to 1000 ºC. This turning point at 600 ºC in micro-PL is different from that at 800 ºC in macro-PL. It is noted that the ZnO component can well crystallize at 600 ºC. This difference suggests that in the inner part, ZnO micro-crystals begin to separate from ZrO_2 at this temperature, which will increase the stress in the samples, and leading to the increase of B-V_Os. As shown in Fig. 2(d), the 800-ºC samples seem to be solid, but contain large numbers of micro-pores. This suggests that in the inner part, the ZnO and ZrO_2 are well separated from each other, and most the stress is concentrated on the surface layers, results in the higher B-V_O density.

5) Concentration quenching effect

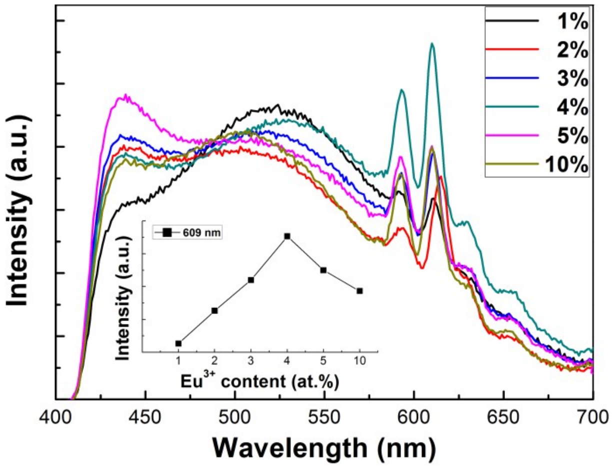

Figure S6 Macro PL of ZrO_2/ZnO: Eu^{3+} composites with different Eu^{3+} ion contents.

References:

1. A. Panwar and K. L. Yadav, *Mater. Lett.*, 2015, **142**, 30-34.

2. Y. Cong, B. Li, S. Yue, D. Fan and X. J. Wang, *J. Phys. Chem. C*, 2009, **113**, 13974-13978.

3. E. Fernandez Lopez, V. Sanchez Escribano, M. Panizza, M. M. Carnasciali and G. Busca, *J. Mater. Chem.*, 2001, **11**, 1891-1897.

4. D. A. Zyuzin, S. V. Cherepanova, E. M. Moroz, E. B. Burgina, V. A. Sadykov, V. G. Kostrovskii and V. A. Matyshak, *J. Solid State Chem.*, 2006, **179**, 2965-2971.

5. S. M. Chang and R. A. Doong, *J. Phys. Chem. B*, 2006, **110**, 20808-20814.

6. X. Qu, H. Song, G. Pan, X. Bai, B. Dong, H. Zhao, Q. Dai, H. Zhang, R. Qin and S. Lu, *J. Phys. Chem. C*, 2009, **113**, 5906-5911.

7. Y. Liu, H. Zhang, X. An, C. Gao, Z. Zhang, J. Zhou, M. Zhou and E. Xie, *J. Alloy Compd.*, 2010, **506**, 772-776.

8. Y. Z. Zhang, Y. X. Liu, X. D. Li, Q. J. Wang and E. Q. Xie, *Nanotechnology*, 2011, **22**, 415702

9. Y. Z. Xie, Z. W. Ma, L. X. Liu, Y. R. Su, H. T. Zhao, Y. X. Liu, Z. X. Zhang, H. G. Duan, J. A. Li and E. Q. Xie, *Appl. Phys. Lett.*, 2010, **97**, 141916

10. J. Zhou, X. Xu, X. Song, Z. Chen, M. Zhou, C. Chen, Y. Liu, J. Song and E. Xie, *J. Mater. Res.*, 2010, **25** 1041-1048.

11. L. R. Singh, *Materials Sciences and Applications*, 2015, **6**, 269-278.

12. D. Wang, G. Xing, M. Gao, L. Yang, J. Yang and T. Wu, *J. Phys. Chem. C*, 2011,

115, 22729-22735.

13. Y. Y. Tay, T. T. Tan, F. Boey, M. H. Liang, J. Ye, Y. Zhao, T. Norby and S. Li, *Physical Chemistry Chemical Physics*, 2010, **12**, 2373-2379.
14. K. Dileep, L. S. Panchakarla, K. Balasubramanian, U. V. Waghmare and R. Datta, *J. Appl. Phys.*, 2011, **109**, 063523.
15. S. Bayan and D. Mohanta, *J. Appl. Phys.*, 2010, **108**, 023512.
16. Y.-P. Du, Y.-W. Zhang, L.-D. Sun and C.-H. Yan, *J. Phys. Chem. C*, 2008, **112**, 12234-12241.
17. R. Chen, Y. Q. Shen, F. Xiao, B. Liu, G. G. Gurzadyan, Z. L. Dong, X. W. Sun and H. D. Sun, *J. Phys. Chem. C*, 2010, **114**, 18081-18084.
18. S. Stojadinović and R. Vasilić, *J. Lumin.*, 2016, **176**, 25-31.
19. G. K. Sidhu, A. K. Kaushik, S. Rana, S. Bhansali and R. Kumar, *Appl. Surf. Sci.*, 2015, **334**, 216-221.
20. S. V. Nikiforov, V. S. Kortov, M. G. Kazantseva and K. A. Petrovykh, *J. Lumin.*, 2015, **166**, 111-116.
21. T. V. Perevalov, D. V. Gulyaev, V. S. Aliev, K. S. Zhuravlev, V. A. Gritsenko and A. P. Yelisseyev, *J. Appl. Phys.*, 2014, **116**, 244109.
22. I. Villa, A. Vedda, M. Fasoli, R. Lorenzi, N. Kränzlin, F. Rechberger, G. Ilari, D. Primc, B. Hattendorf, F. J. Heiligtag, M. Niederberger and A. Lauria, *Chem. Mater.*, 2016, **28**, 3245-3253.
23. S. Gao, H. Zhang, R. Deng, X. Wang, D. Sun and G. Zheng, *Appl. Phys. Lett.*, 2006, **89**, 123125.
24. C. Park, J. Lee and W. S. Chang, *J. Phys. Chem. C*, 2015, **119**, 16984-16990.
25. Y. Z. Zhang, Y. P. Liu, L. H. Wu, E. Q. Xie and J. T. Chen, *J. Phys. D*, 2009, **42**.